Published in final edited form as:
Heart Rhythm. 2012 January ; 9(1): 134–142. doi:10.1016/j.hrthm.2011.08.029.

Profile of L-type Ca^{2+} current and Na^+/Ca^{2+} exchange current during cardiac action potential in ventricular myocytes

Tamas Banyasz, M.D. Ph.D.[1,2], **Balazs Horvath, M.D. Ph.D.**[1], **Zhong Jian, Ph.D.**[1], **Leighton T. Izu, Ph.D.**[1], and **Ye Chen-Izu, Ph.D.**[1,3,4]

[1]Department of Pharmacology, University of California, Davis, USA

[2]Department of Physiology, University of Debrecen, Hungary

[3]Department of Biomedical Engineering, University of California, Davis

[4]Department of Internal Medicine, Division of Cardiology, University of California, Davis

Abstract

Objective—The L-type Ca^{2+} current ($I_{Ca,L}$) and the Na^+/Ca^{2+} exchange current (I_{NCX}) are major inward currents that shape the cardiac action potential (AP). Previously, the profile of these currents during AP was determined from voltage-clamp experiments that used Ca^{2+} buffer. In this study, we aimed to obtain direct experimental measurement of these currents during cardiac AP with Ca^{2+} cycling.

Method—A newly developed AP-clamp sequential dissection method was used to record ionic currents in guinea pig ventricular myocytes under a triad of conditions: using the cell's own AP as the voltage command, using internal and external solutions that mimic the cell's ionic composition and, importantly, no exogenous Ca^{2+} buffer was used.

Results—The nifedipine-sensitive current (I_{NIFE}), which is composed of $I_{Ca,L}$ and I_{NCX}, revealed hitherto unreported features during AP with Ca^{2+} cycling in the cell. We identified two peaks in the current profile followed by a long residual current extending beyond the AP, coinciding with a residual depolarization. The second peak and the residual current become apparent only when Ca^{2+} is not buffered. Pharmacological dissection of I_{NIFE} using SEA0400 shows that $I_{Ca,L}$ is dominant during phase-1&2 whereas I_{NCX} contributes significantly to the inward current at phase-3&4 of AP.

Conclusion—These data provide the first direct experimental visualization of $I_{Ca,L}$ and I_{NCX} during cardiac AP and Ca^{2+} cycle. The residual current reported here can serve as a potential substrate for afterdepolarizations when increased under pathologic conditions.

Keywords

Cardiac; ventricular; myocyte; action potential; L-type Ca^{2+} channel; Na^+/Ca^{2+} exchanger; arrhythmia

Correspondence: Ye Chen-Izu Ph.D., Assistant Professor, Department of Pharmacology, University of California, Davis, 2221 Tupper Hall, 451 Health Science Drive, Davis, CA 95616, USA, Phone: (530) 752-3232, ychenizu@ucdavis.edu.

Conflict of Interest: none.

Introduction

The L-type Ca^{2+} current ($I^{Ca,L}$) and the Na^{+}/Ca^{2+} exchange current (I_{NCX}) are two major inward currents that provide the depolarization drive to shape action potential (AP) plateau and repolarization phase in cardiac myocytes. Changes in the magnitude or timing of these currents could cause development of cardiac arrhythmias. Hence, understanding the dynamic properties of these currents during the AP cycle is of great interest. However, the current knowledge on the $I_{Ca,L}$ and I_{NCX} during AP has been largely based on model simulations derived from traditional voltage-clamp data. Previous voltage-clamp experiments often used simplified ionic solutions to isolate the currents and used exogenous Ca^{2+} buffer—conditions that differ from physiological milieu. In this study, we directly measured the ionic currents during AP under a triad of conditions mimicking physiological environment: (1) the cell's own AP was recorded and used as command voltage to directly record the $I_{Ca,L}$ and I_{NCX} during AP; (2) the physiological ionic compositions were used in both the internal and the external solutions; and (3) the intracellular Ca^{2+} cycling during AP was preserved by not using exogenous Ca^{2+} buffer in the internal solution.

We recorded the nifedipine-sensitive current (I_{NIFE}), which is the composite current of $I_{Ca,L}$ and I_{NCX}, during AP with Ca^{2+} cycling. Then we used a newly developed AP-clamp Sequential Dissection technique ('Onion-Peeling')[1] to separate $I_{Ca,L}$ and I_{NCX} using nifedipine and SEA0400. This novel experimental approach allows us, for the first time, to directly visualize the dynamics of $I_{Ca,L}$ and I_{NCX} currents during AP with Ca^{2+} cycling in the cell. Our data reveal novel and distinctive features of I_{CaL} and I_{NCX} that occur when the cell is most vulnerable to early or delayed afterdepolarizations. Measurement of the currents during the AP with Ca^{2+} cycling under physiological conditions also provide realistic data to aid computational modeling and rational design of effective drug therapies for treating cardiac arrhythmias.

Methods

All laboratory procedures conform to the *Guide for the Care and Use of Laboratory Animals* published by the US National Institutes of Health.

Cell isolation

Hartley guinea pigs (male, 3–4 month old, purchased from Charles River Laboratories USA), were first injected with heparin (800u, I.P.) and then anesthetized with nembutal (100 mg/kg, I.P.). After achieving deep anesthesia to suppress spinal cord reflexes, a standard enzymatic technique was used to isolate ventricular myocytes. [2]

Electrophysiology

AP-clamp Sequential Dissection experiments were conducted as described in our previous publication[1]. Cells were continuously superfused with a modified Tyrode solution (BTy) containing (in mmol/L) NaCl 120, KCl 5, $CaCl_2$ 2, $MgCl_2$ 1, HEPES 10, $NaHCO_3$ 25, Glucose 10, pH 7.3. The pipette solution contained (in mmol/L) K-Aspartate 115, KCl 45, Mg-ATP 3, HEPES 5, cAMP 0.1, pH 7.25. Depending on the experiment, 0, 2 or 10 mM EGTA was added into the pipette solution. Basic experimental steps: (1) Record the steady state AP under I-clamp (I=0) at 1 Hz pacing frequency. (2) Apply this AP as the voltage command onto the same cell under V-clamp at 1 Hz. The net current output, $\boldsymbol{I_{BG}}$ should be zero. (3) Isolate the current of interest by using its specific blocker to remove it from the net current output, $\boldsymbol{I_{drug}}$. (4) The current of interest is then obtained by subtraction: $\boldsymbol{I = I_{BG} - I_{drug}}$. (5) Next, isolate the 2nd current of interest by applying the 2nd channel blocker, and then obtained the 2nd current by subtraction: $\boldsymbol{I_2 = I_{drug1} - I_{drug2}}$. Repeat (5) to isolate the

3rd, the 4th, and more currents by sequentially adding the specific blocker for each channel (Table-1). The currents were recorded after they reached steady state. The inhibitory coefficient of SEA0400 on blocking I_{NCX} was measured using a standard ramp V-clamp protocol [3]. The inhibitory coefficient of SEA0400 on blocking I_{CaL} was measured using a standard V-clamp protocol [2].

All experiments were conducted at 21±1°C, except those in Fig.6 were conducted at 36±0.5°C. Chemicals were purchased from SIGMA-ALDIRCH (USA), except SEA0400, 2-[4-[(2,5-difluorophenyl)methoxy]phenoxy]-5-ethoxyaniline was provided by Taisho Pharmaceutical (Japan).

Results

Nifedipine-sensitive current during AP with Ca^{2+} cycling

Ionic currents were recorded in ventricular cardiac myocytes using the Onion-Peeling technique. First, we tested the effect of 0.1% DMSO which is used as solvent of drugs. Application of DMSO resulted in no change in the zero baseline current (Fig.1A). Nifedipine at 10 μM concentration was added into the bath to dissect out I_{NIFE}, as shown in Fig.1B. I_{NIFE} displays several distinct features. There is a steep rise of the current at phase-1 of AP, which we named the *initial current* ("*I*") and measured it at 10 ms following the AP upstroke. During phase-2, the current slows down and forms a dome, which we named the *dome current* and measured it at APD10 (early plateau "*E*") and APD20 (dome "*D*") (APD# is defined as the AP duration measured at #% repolarization.) During phase-3, the current declines but then resurges to reach a second dome ("*S*"). Then the current declines again and slowly diminishes during phase-4; we named this feature the *residual current* ("*R*") and measured it at 30 ms after $-V_{max}$ (the maximum repolarization rate of AP during phase-3). While the initial phase and the dome features were seen before [45], the second dome and the residual current during AP phase-3&4 are novel observations that had not been reported previously.

To confirm that I_{NIFE} originates from blocking the L-type Ca^{2+} channel, we used a different blocker, nisoldipine 1 μM to record the nisoldipine-sensitive current (I_{NISO}) under AP-clamp. I_{NISO} (Fig.1C, n=8 cells) displays the same distinct features and similar values as I_{NIFE} (Fig.1D, n=8 cells).

Corresponding to the residual current, we also found a slowing down of the membrane repolarization at the end of AP that extends beyond APD95 (Fig.1E), which we named *residual depolarization* and measured it as the voltage above the resting potential at 30 ms after $-V_{max}$ (the same time point for measuring the residual current). The residual depolarization had not been reported in the literature. However, we have consistently found this residual depolarization in both the single cell and the ventricular tissue (using sharp electrode recording of AP, data not shown), confirming its existence *in vivo*. Furthermore, the residual depolarization shows a strong positive correlation with the residual current (Fig. 1F), indicating a connection between the two.

I_{NIFE} consists of $I_{Ca,L}$ and I_{NCX}

I_{NIFE} is composed of not only $I_{Ca,L}$ but also I_{NCX} and other Ca^{2+} sensitive currents. This is because blocking $I_{Ca,L}$ also eliminates Ca^{2+} entry into the cell to trigger SR Ca^{2+} release, which abolishes the intracellular Ca^{2+} transient and its associated currents such as the inward I_{NCX}, the Ca^{2+}-activated Cl^- current, and possibly a fraction of K^+ currents that is sensitive to Ca^{2+}. We conducted all experiments at 21°C to render the Cl^- current negligible.[67] To determine the Ca^{2+} sensitivity of K^+ currents, we used the Onion-Peeling method [1] to record I_{Ks}, I_{Kr}, I_{K1}, and I_{NIFE} in the same cell. The currents measured with Ca^{2+}

cycling versus with EGTA are listed in Table-1. I_{K1} and I_{Ks} did not show any significant difference in the peak current density; peak I_{Kr} decreased slightly (0.15 A/F). However, the average peak current of I_{NIFE} was 1.4 A/F with Ca^{2+} cycling and 2.4 A/F with EGTA. Hence, the Ca^{2+} sensitive component in K^+ currents is much smaller than the magnitude of I_{NIFE}, which should cause only a slight underestimation of I_{NIFE}. Therefore, the I_{NIFE} recorded in our experiment is mainly composed of $I_{Ca,L}$ and I_{NCX}.

The Ca^{2+}-dependent features of I_{NIFE}

To separate the $I_{Ca,L}$ and I_{NCX} components in I_{NIFE}, we added 10 mM EGTA to the pipette solution to buffer intracellular Ca^{2+} and minimize the inward I_{NCX}. A typical recording of I_{NIFE} with 10 mM EGTA is shown in Fig.2A. Now the I_{NIFE} profile displays the *initial* current and the *dome* current features, but without any discernable *second dome* and *residual current*, different from that recorded with Ca^{2+} cycling (Fig.1B). Moreover, the residue depolarization is also eliminated (Fig.2B).

When EGTA concentration in the pipette was reduced from 10 mM to 2 mM, I_{NIFE} displayed the initial current and the dome current but the second dome was absent in all records. Buffering of Ca^{2+} eliminated the second dome and the residual current, but elevated the dome current in concentration-dependent manner (Fig.2A&C). These phenomena are visualized in the I–V relationship (Fig.2D) and confirmed in the statistical comparison of the current amplitudes along the AP time course (Fig.2E). Again, corresponding to a lack of the residual current the residual depolarization was also eliminated (Fig.2F). Note that low EGTA (2 mM) buffering can significantly affect Ca^{2+} and the dynamics of I_{NIFE} during AP.

Contribution of I_{NCX} to I_{NIFE}

The fact that buffering Ca^{2+} can eliminate the second dome and the residual current suggests that I_{NCX} might contribute to these features. To investigate this we used an I_{NCX} inhibitor, SEA0400 at 3 μM concentration to record the SEA-sensitive current (I_{SEA}). As shown in Fig.3A, I_{SEA} displays a small initial current at AP phase-1; gradually increases during phase-2, peaks at early phase-3 and declines; the current then turns around and reaches the second dome at late phase-3; and then declines to a residual current extending into phase-4. These data show that I_{NCX} dominates the late phases of AP. After I_{SEA} had developed and stabilized, we added 10 μM nifedipine into the bath and recorded the $I_{SEA+NIFE}$ current (Fig. 3B, C). Statistical comparison of the currents shows that the contribution of I_{NCX} to $I_{SEA+NIFE}$ is relatively small during the early phases of AP but becomes larger in later phases (Fig.3D).

Although SEA0400 is the most potent inhibitor of I_{NCX} currently available, it also partially blocks $I_{Ca,L}$. This means that I_{SEA} is composed of not only I_{NCX} but also a small portion of $I_{Ca,L}$. To separate I_{NCX} from $I_{Ca,L}$, we measured the inhibitory coefficients of 3 μM SEA0400 on I_{NCX} and $I_{Ca,L}$, respectively. The inhibitory effect of SEA0400 on I_{NCX} is voltage-dependent, about 65% and 51% for the outward I_{NCX} measured at +30 mV and the inward I_{NCX} measured at - 75 mV (Fig.3E, F). The inhibitory effect of 3 μM SEA0400 on I_{CaL} is about 24% at the peak and is also voltage-dependent (Fig.3G, H).

Reconstruction of $I_{Ca,L}$ and I_{NCX} during AP

Both I_{CaL} and I_{NCX} are heavily dependent on the local Ca^{2+} concentration. However, currently there is no available technique to *directly* measure the local Ca^{2+} concentrations sensed by the channel/transporter. To circumvent this problem, we took a simple approach to calculate I_{CaL} and I_{NCX} from the paired recordings of I_{SEA} and $I_{SEA+NIFE}$ (using two equations to solve for two unknowns) by utilizing the differential inhibitory coefficients of SEA versus nifedipine. This simple calculation using paired recordings provides a somewhat

direct approach to disentangle I_{CaL} and I_{NCX} Given that I_{CaL} and I_{NCX} are the predominant currents blocked by nifedipine and SEA0400, the charge conservation gives the following equations:

$$I_{SEA+NIFE} = I_{CaL} + \alpha I_{NCX}$$
$$I_{SEA} = k_{CaL}(I_{CaL} + \alpha I_{NCX}) + k_{NCX}(1 - \alpha k_{CaL}) I_{NCX}$$

where k_{CaL} and k_{NCX} are the voltage-dependent inhibitory coefficients of I_{CaL} and I_{NCX} measured from the voltage-clamp experiments shown in Fig.3F&H. α is a scaling factor (ranging between 0 and 1 inclusive) that reflects the portion of I_{NCX} that is affected by changes in I_{CaL}). Because the local Ca^{2+} concentration sensed by the Na^+/Ca^{2+} exchanger is unknown, we therefore solved the equations for α =0 and 1 to calculate the boundary conditions and estimate the currents. Fig.4 show I_{NCX} and I_{CaL} computed from paired recordings of I_{SEA} and $I_{SEA+NIFE}$ during AP with Ca^{2+} cycling (Column A) or with EGTA (Column B). The current traces are shown in the upper row. Notice that I_{SEA} is an inward current due to the forward mode *I*NCX when Ca^{2+} is cycling, but turns into an outward current due to the reverse mode I_{NCX} when Ca^{2+} is buffered with 10 mM EGTA. The $I_{Ca,L}$ and I_{NCX} calculated from I_{SEA} and $I_{SEA+NIFE}$ are shown in Fig.4 (middle and lower row). The blue (α =1) and red (α =0) traces demarcate the upper and the lower boundaries of the currents, respectively. The actual current should fall within the boundaries. Note that I_{NCX} is bounded within a narrow range; hence the profile of I_{NCX} during AP is clearly defined. A probable profile of the current is highlighted with black line (calculated as an intermediate state with α=0.8).

The magnitude of I_{CaL} dome current is about 0.3 A/F when Ca^{2+} is normally cycling (Column A, middle panel), but becomes much greater to about 2 A/F when Ca^{2+} is buffered (Column B, middle panel). This difference reflects a profound influence of the Ca^{2+}-dependent inactivation of $I_{Ca,L}$. Note also that buffering Ca^{2+} completely eliminated the second dome and the residual current. When Ca^{2+} is cycling, I^{NCX} is briefly outward at the beginning of AP but soon becomes an inward current (Column A, lower panel), and reaches a peak of about 0.2 A/F. In contrast, when Ca^{2+} is buffered, I_{NCX} is always outward during AP (Column B, lower panel).

Effects of SEA0400

It has been proposed that inhibiting I_{NCX} might provide an effective therapy for some forms of arrhythmias. We predicted that using SEA0400 to treat the cell would reduce the dome current and the residual current. To test this, we pretreated cells with 3 μM SEA0400 and recorded the remaining I_{NIFE} under AP-clamp. As shown in Fig.5A, SEA0400 treatment shortened APD, in consistent with its effect on reducing the dome and the residual current.

A representative trace of the I_{NIFE} in the SEA0400 pretreated cell is shown in Fig.5B. Recall that in the control cell (Fig.1B) the dome is larger than the initial current, here in the SEA0400 pretreated cell the dome becomes smaller than the initial current, indicating a portion of the dome current is contributed by the inward I_{NCX}. The residual current is significantly smaller after SEA0400 treatment (Fig.5C), in consistent with the I_{NCX} contribution. Meanwhile the residual depolarization is also smaller (Fig.5D). In fact, a positive correlation between the residual current and the residual depolarization exists universally for all the experimental conditions tested (Fig.5E), indicating that the residual current is responsible for the residual depolarization.

I_{NIFE} at body temperature

To establish the physiological relevance of our new findings, we also conducted AP-clamp experiments at body temperature. The I_{NIFE} at 36°C displays essentially the same features (Fig.6A). The Second dome and the residual currents are prominent, and the residual depolarization is also present (Fig.6B). The insert shows the Ca^{2+} transient measured with Fura-2. Using EGTA to buffer Ca^{2+} eliminates the residual current (Fig.6C) and the residual depolarization (Fig.6D). Statistical comparison show that with Ca^{2+} cycling, the dome currents is significant smaller (Fig.6E) due to Ca^{2+} -dependent inactivation of $I_{Ca,L}$ (CDI), but the residual current and the residual depolarization are significantly larger (Fig.6E,F) due to the inward I_{NCX}.

Discussion

Here we present experimental measurements of $I_{Ca,L}$ and I_{NCX} currents during the action potential with Ca^{2+} cycling in ventricular myocytes. This was enabled by a triad of conditions: (1) using the cell's own AP as the voltage command; (2) using the internal and external solutions that mimic the physiological milieu; and (3) Ca^{2+} cycling during AP was preserved by not using exogenous Ca^{2+} buffer. To the best of our knowledge, it is the first time this triad of conditions has been used to record the ionic currents during cardiac AP with Ca^{2+} cycling.

I_{NIFE} was obtained by blocking L-type Ca^{2+} current under AP-clamp. However, blocking Ca^{2+} current also affects other Ca^{2+} dependent currents including I_{NCX}, Ca^{2+}-activated Cl^- current, and the Ca^{2+} sensitive components in K^+ currents. The Cl^- current was rendered negligible by conducting experiments at 21°C.[67] We also found no significant contributions of K^+ currents. Hence, I_{NIFE} mainly consists of $I_{Ca,L}$ and I_{NCX}. The profile of I_{NIFE} during AP exhibits distinct features: an *initial* current at phase-1, a *dome* at phase-2, a resurging *second dome* at phase-3 and a *residual* current at phase-4. The second dome and the residual current had not been reported before; these novel features become apparent only when Ca^{2+} is not buffered. We also detected a hitherto unreported residual depolarization at the end of AP which can be attributed to the residual current. Furthermore, we found that $I_{Ca,L}$ contributes predominantly to the initial and the dome current whereas I_{NCX} contributes significantly to the second dome and the residual current. The timing and magnitude of these currents suggest their relative roles in shaping the AP profile and generating early or delayed afterdepolarizations.

The dynamic profile of $I_{Ca,L}$ during cardiac AP and its contribution to afterdepolarizations has been under active investigation. Previous studies used variants of the AP-clamp technique and reported the initial current and the dome current features, but never before reported the second dome and the residual current features. This discrepancy can be explained by the experimental conditions used in those studies that differed from the triad of conditions used in our experiments. First, in earlier studies the AP waveform used as voltage command was either a representative AP [5] or a reconstructed AP [8], which does not, in general, match each cell's unique AP. Hence the current profile would be distorted from its natural state in the cell. Second, earlier experiments used non-physiological solutions (substituting Na^+ and K^+), but ion species and concentration are known to alter the Ca^{2+} channel kinetics. [910] Third, most earlier experiments used exogenous Ca^{2+} buffer, and the $I_{Ca,L}$ profile reported in those studies [1185] are similar to the I_{NIFE} profile recorded with EGTA in our study (Fig.2A&C). The second dome and the residual current in I_{NIFE} are novel features revealed only under the triad of conditions used in our AP-clamp experiments.

The dynamic profile of $I_{Ca,L}$ during AP is determined by an interplay between the changing driving force during AP and CDI. Importantly, our data show a significant modulation of $I_{Ca,L}$ during AP by CDI, seen as the I_{NIFE} dome current increases with EGTA in a dose-dependent manner (Fig.2E). The average dome current is 1.4 pA/pF when Ca^{2+} is cycling, and increases to 2.4 pA/pF when Ca^{2+} is buffered with10 mM EGTA. It is noteworthy that previous voltage-clamp and AP-clamp studies (using Ca^{2+} buffer) reported a peak $I_{Ca,L}$ between 2–10 pA/pF [1154]; quantitative models based on those data also had a peak $I_{Ca,L}$ in that range [12]. Our data show a much smaller $I_{Ca,L}$ magnitude in the cell measured under AP-clamp with Ca^{2+} cycling, and provide realistic experimental data for future modeling considerations.

Previously, a lack of selective blocker prevented direct measurement of I_{NCX} [13]. In this study we used SEA0400 paired with nifedipine to isolate the I_{NCX} during AP with Ca^{2+} cycling. Our data reveal that I_{NCX} presents an outward current at the beginning of AP, which turns into a small inward current at early phase-2; the inward I_{NCX} increases and contributes significantly to the I_{NIFE} second dome and the residual current at phase-3&4. In comparison to earlier studies, Grantham and Cannell [5] had calculated an I_{NCX} profile that showed a large outward current throughout AP phase-1&2, then turned into an inward current at phase-3, and then peaked at the end of phase-3. Weber et al. [14] reconstructed the I_{NCX} during AP by correlating the Ca^{2+} transient with the steady-state I_{NCX} measurements at various Ca^{2+} concentrations. They showed that, in rabbit ventricular myocytes, I_{NCX} was a rapid outward current at phase-1, turned to inward at early phase-2, reached a peak at the end of phase-3, and then slowly declined during phase-4. The I_{NCX} profile in Fig.4 (Column A, lower panel) shows similar features as their result, but differs in the time course and the magnitude of current. Given the importance of I_{NCX} in shaping AP, our AP-clamp measurement of I_{NCX} in physiological milieu provides important data for developing more accurate quantitative models.

Increased $I_{Ca,L}$ or I_{NCX} had been found to induce afterdepolarizations [1516]. Inhibiting $I_{Ca,L}$ with Ca^{2+} channel blocker effectively eliminated early afterdepolarizations. [15, 17, 18] Inhibiting I_{NCX} with SEA0400 also effectively reduced early and delayed afterdepolarizations. [313] Hence, $I_{Ca,L}$ and I_{NCX} have been proposed as therapeutic targets for treating cardiac arrhythmias (see review by Sipido et al. [13]). The relative contributions of $I_{Ca,L}$ and I_{NCX} to the depolarization drive are resolved in the current study. As we observed, $I_{Ca,L}$ is the dominant inward current during AP phase-1&2, whereas I_{NCX} is the dominant inward current during phase-3&4. Both $I_{Ca,L}$ and I_{NCX} contribute to the dome current, the second dome, and the residual current. Given the intertwined nature of $I_{Ca,L}$ and I_{NCX}, it is the combination of these two currents, not just one or the other, determines the total depolarization drive that shapes AP profile and afterdepolarizations. [19] Importantly, the newly observed second dome and the residual current occurring at phase-3&4 have the right timing and the shape to generate afterdepolarizations if not counterbalanced by repolarization currents. Our data clearly show that the second dome coincides with the vulnerable phase of AP where early afterdepolarizations may develop, while delayed afterdepolarizations may occur at where we observed the residual current. The current study provides useful and physiologically relevant data to aid quantitative modeling of cardiac AP and rational design of anti-arrhythmia drug therapies.

Acknowledgments

We thank Shaden Khabbaz, Charles Payne, and Stephanie E. Edelmann for their excellent work in isolating cardiac cells. We are grateful to Dr. Robert Hadley (University of Kentucky) for kindly providing cells for our early experiments. We are also grateful to Drs. Donald M Bers and Kenneth Ginsburg and Taisho Pharmaceutical (Tokyo, Japan) for the generous gift of SEA0400. Our gratitude also goes to Dr. Donald M Bers (University of

California, Davis) and Dr. Mark E Anderson (University of Iowa) for reading early manuscripts and contributing insightful comments.

Funding: This work was supported by NIH R01 grant (HL90880) to LTI, YC and TB, NIH R03 grant (AG031944) to YC, American Heart Association National Center Scientist Development Award (0335250N) to YC, European Society of Cardiology Visiting Scientist Award to BH, and funds from the University of California to LTI and YC.

References

1. Banyasz T, Horvath B, Jian Z, Izu LT, Chen-Izu Y. Sequential dissection of multiple ionic currents in single cardiac myocytes under action potential-clamp. J Mol Cell Cardiol. 2011; 50(3):578–581. [PubMed: 21215755]
2. Chen-Izu Y, Chen L, Banyasz T, et al. Hypertension-induced remodeling of cardiac excitation-contraction coupling in ventricular myocytes occurs prior to hypertrophy development. Am J Physiol Heart Circ Physiol. 2007; 293:H3301–H3310. [PubMed: 17873027]
3. Birinyi P, Acsai K, Banyasz T, et al. Effects of SEA0400 and KB-R7943 on Na+/Ca2+ exchange current and L-type Ca2+ current in canine ventricular cardiomyocytes. Naunyn Schmiedebergs Arch Pharmacol. 2005; 372(1):63–70. [PubMed: 16086157]
4. Linz KW, Meyer R. Profile and kinetics of L-type calcium current during the cardiac ventricular action potential compared in guinea-pigs, rats and rabbits. Pflügers Archiv European Journal of Physiology. 2000; 439(5):588–599.
5. Grantham CJ, Cannell MB. Ca2+ Influx During the Cardiac Action Potential in Guinea Pig Ventricular Myocytes. Circulation Research. 1996; 79(2):194. [PubMed: 8755995]
6. Nakajima I, Watanabe H, Iino K, Saito T, Miura M. Ca2+ overload evokes a transient outward current in guinea-pig ventricular myocytes. Circ J. 2002; 66(1):87–92. [PubMed: 11999672]
7. Puglisi JL, Yuan W, Bassani JWM, Bers DM. Ca2+ Influx Through Ca2+ Channels in Rabbit Ventricular Myocytes During Action Potential Clamp: Influence of Temperature. Circ Res. 1999; 85(6):e7–e16. [PubMed: 10488061]
8. Linz KW, Meyer R. Control of L-type calcium current during the action potential of guinea-pig ventricular myocytes. J Physiol. 1998; 513(2):425–442. [PubMed: 9806993]
9. Linz KW, Meyer R. Modulation of L-type calcium current by internal potassium in guinea pig ventricular myocytes. Cardiovasc Res. 1997; 33(1):110–122. [PubMed: 9059534]
10. Hess P, Lansman JB, Tsien RW. Calcium channel selectivity for divalent and monovalent cations. Voltage and concentration dependence of single channel current in ventricular heart cells. J Gen Physiol. 1986; 88(3):293–319. [PubMed: 2428919]
11. Arreola J, Dirksen RT, Shieh RC, Williford DJ, Sheu SS. Ca2+ current and Ca2+ transients under action potential clamp in guinea pig ventricular myocytes. Am J Physiol. 1991; 261:C393–C397. [PubMed: 1651654]
12. Faber GM, Silva J, Livshitz L, Rudy Y. Kinetic properties of the cardiac L-type Ca2+ channel and its role in myocyte electrophysiology: a theoretical investigation. Biophys J. 2007; 92(5):1522–1543. [PubMed: 17158566]
13. Sipido KR, Bito V, Antoons G, Volders PG, Vos MA. Na/Ca Exchange and Cardiac Ventricular Arrhythmias. Annals of the New York Academy of Sciences. 2007; 1099:339–348. [PubMed: 17446474]
14. Weber CR, Piacentino V, Ginsburg KS, Houser SR, Bers DM. Na-Ca Exchange Current and Submembrane [Ca2+] During the Cardiac Action Potential. Circ Res. 2002; 90(2):182–189. [PubMed: 11834711]
15. January CT, Riddle JM. Early afterdepolarizations: mechanism of induction and block. A role for L-type Ca2+ current. Circ Res. 1989; 64(5):977–990. [PubMed: 2468430]
16. Pogwizd SM, Qi M, Yuan W, Samarel AM, Bers DM. Upregulation of Na+/Ca2+ Exchanger Expression and Function in an Arrhythmogenic Rabbit Model of Heart Failure. Circ Res. 1999; 85(11):1009–1019. [PubMed: 10571531]
17. Anderson ME, Braun AP, Wu Y, et al. KN-93, an inhibitor of multifunctional Ca/calmodulin-dependent protein kinase, decreases early afterdepolarizations in rabbit heart. J Pharmacol Exp Ther. 1998; 287(3):996–1006. [PubMed: 9864285]

18. Yamada MOK, Niwa A, Tsujino N, Nakada T, Hirose M. Contribution of L-type Ca2+ channels to early afterdepolarizations induced by I Kr and I Ks channel suppression in guinea pig ventricular myocytes. J Membr Biol. 2008; 222(3):151–166. [PubMed: 18566732]

19. Weiss JN, Garfinkel A, Karagueuzian HS, Chen P-S, Qu Z. Early afterdepolarizations and cardiac arrhythmias. Heart Rhythm. 2010; 7(12):1891–1899. [PubMed: 20868774]

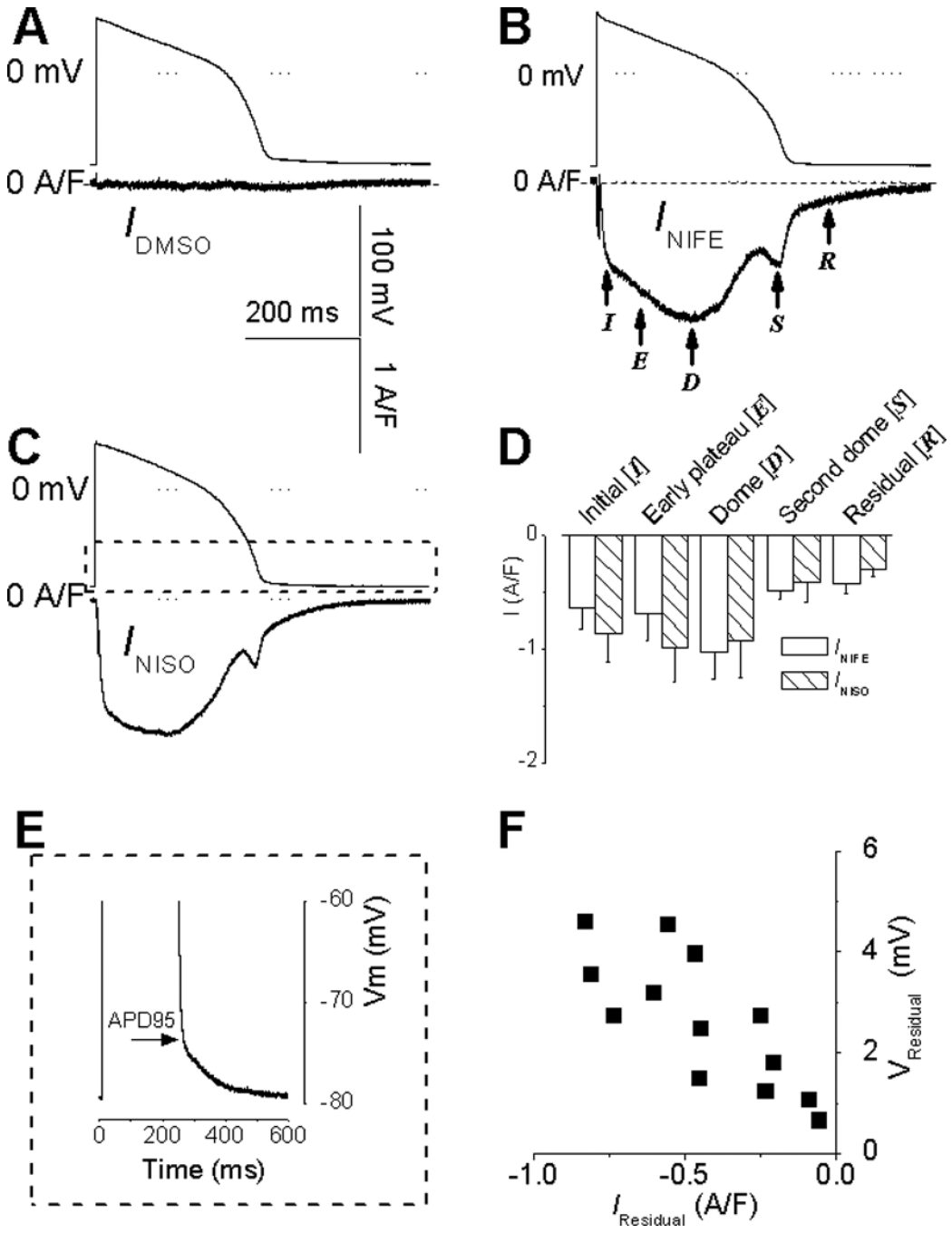

Fig.1.

Panel A shows a representative current trace recorded with 0.1% (v/v) DMSO (used as solvent of channel blockers). The flat "zero current" indicate a lack of any DMSO effect on membrane currents (n=5 cells). Panel B and C are representative recordings of I_{NIFE} or I_{NISO} respectively. Panel D shows the statistical comparison of I_{NIFE} (n=7) and I_{NISO} (n=5), demonstrating no significant differences between the currents. Panel E shows the residual depolarization. Panel F shows a positive correlation between the residual depolarization and the residual current measured at 30 ms after $-V_{max}$.

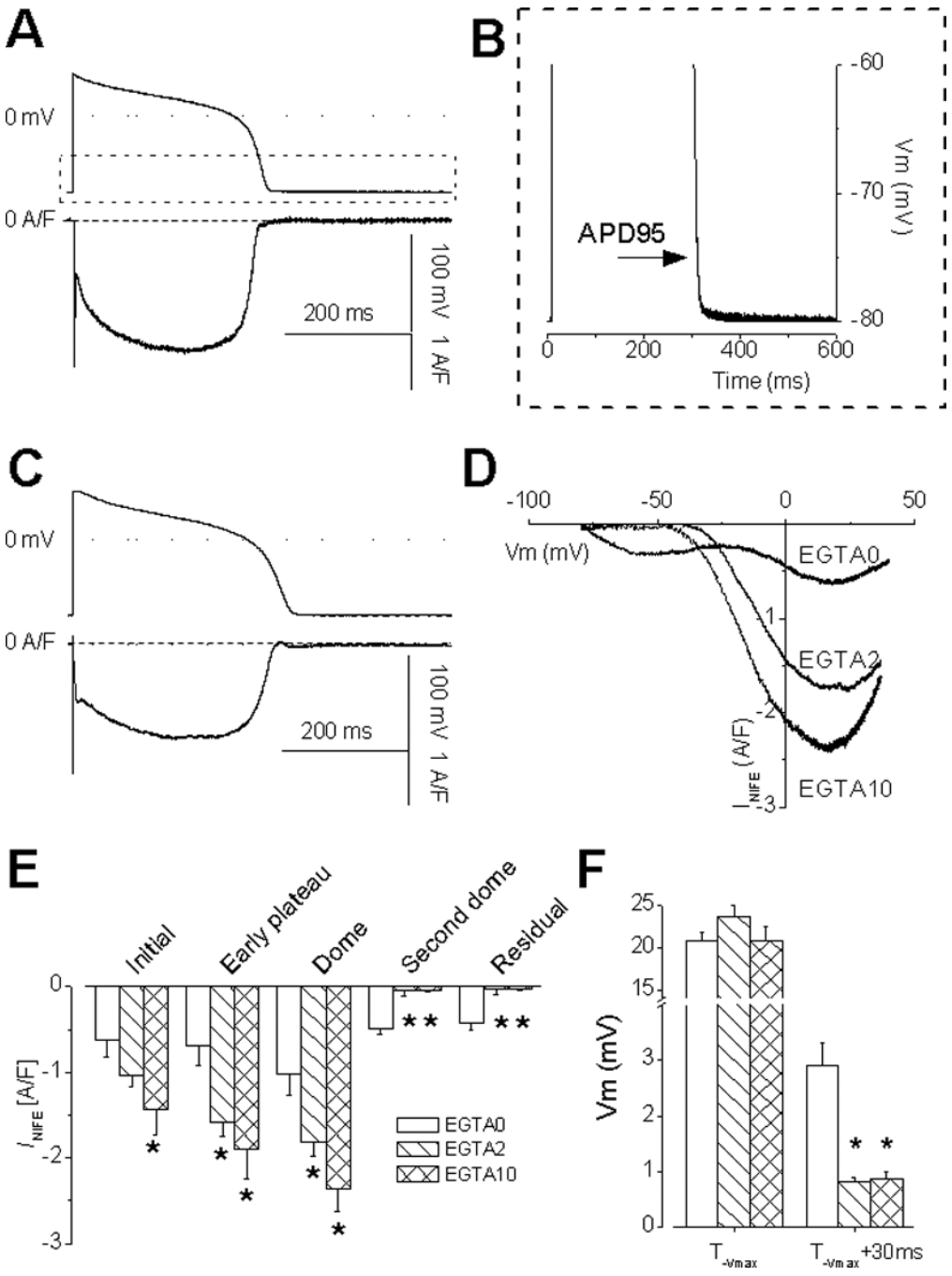

Fig.2.

Representative I_{NIFE} recorded under AP-clamp with 10 mM EGTA in pipette (n=10 cells). Notice an absence of the second dome, the residual current (A), and the residual depolarization (B). I_{NIFE} recorded with 2 mM EGTA (C, n=14 cells), the current-voltage relationship (D), and statistical comparison between different Ca^{2+} buffering conditions (E) show increased current density with more EGTA buffering. Panel F demonstrates that EGTA did not affect the voltage at $-V_{max}$ but significantly reduced the residual depolarization at 30 ms after $-V_{max}$. (t-test, $p<0.05$*; $p<0.01$**)

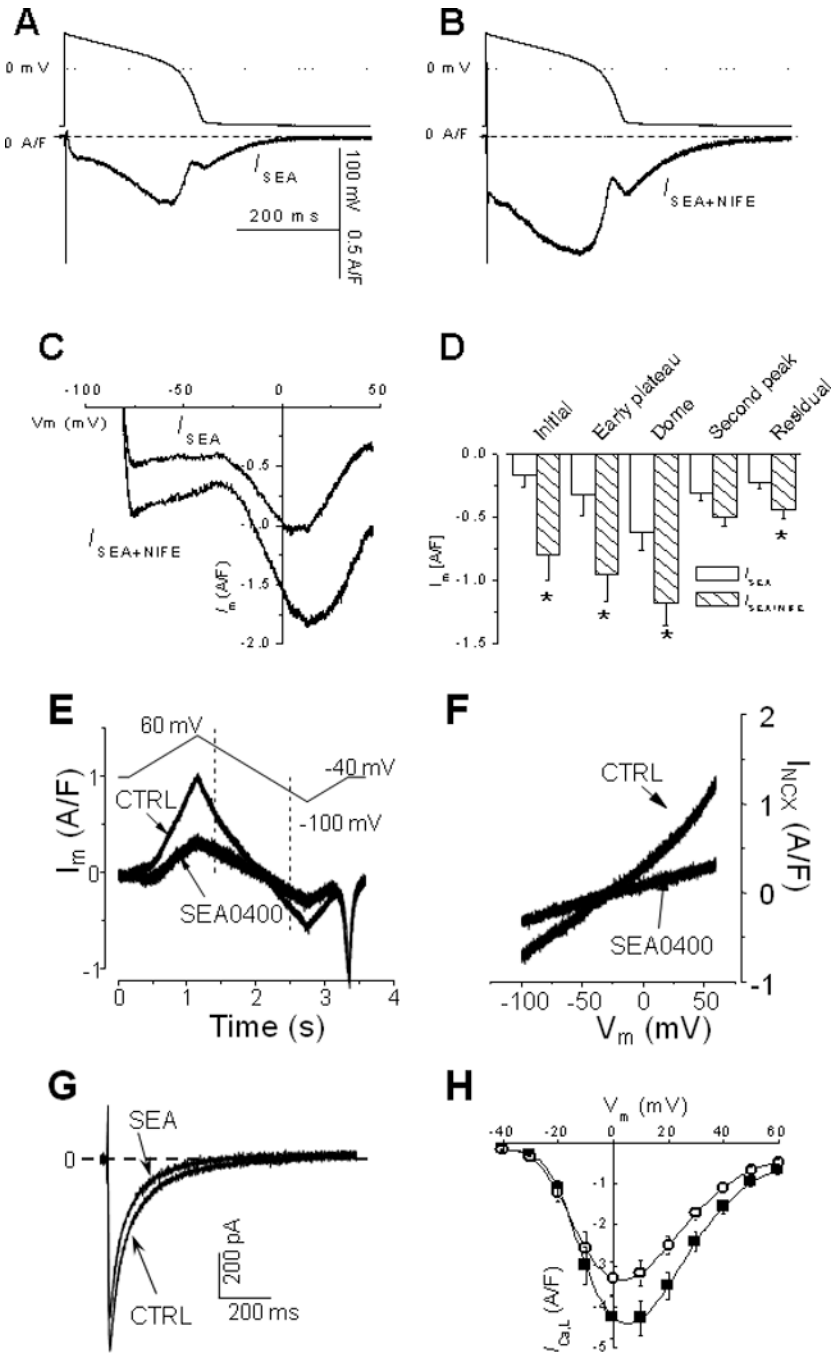

Fig.3.

Panel A shows a representative current recorded with 3 μM SEA0400 (I_{SEA}). When 10 μM nifedipine was added, $I_{SEA+NIFE}$ displays similar characteristics (B). Panel C and D show the instant current-voltage relationship of I_{SEA} and $I_{SEA+NIFE}$ and statistical comparison of data (n=7 cells, t-test, $p<0.05$*). Standard V-clamp protocols were used to measure the inhibitory effects of 3 μM SEA. Panel E and F show current traces and the I–V relationship of I_{NCX} before and after application of SEA. Panel G and H show representative current traces and the I–V relationship of $I_{Ca,L}$ before and after application of SEA.

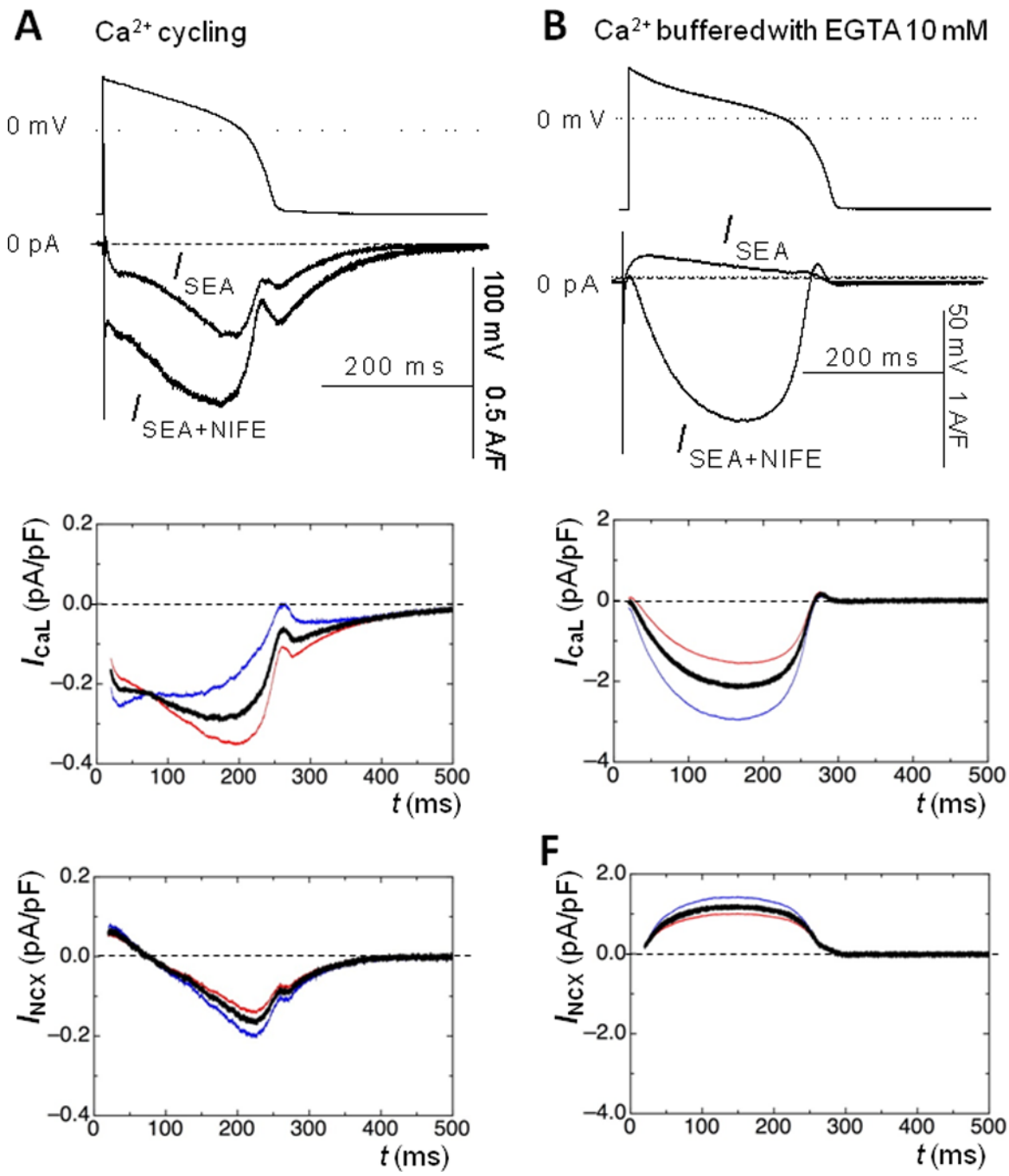

Fig.4.

Column A and B show I_{SEA} and $I_{SEA+NIFE}$ recorded in the absence and presence of EGTA, respectively. EGTA buffering of Ca^{2+} reversed I_{SEA} and amplified $I_{SEA+NIFE}$. Mathematical reconstruction of $I_{Ca,L}$ and I_{NCX} assuming zero coupling (α=0, red line) or linear coupling (α=1, blue line) between $I_{Ca,L}$ and I_{NCX} mark the boundaries of the actual currents. Black line shows an intermediate state (α=0.8), highlighting a probable profile of the currents.

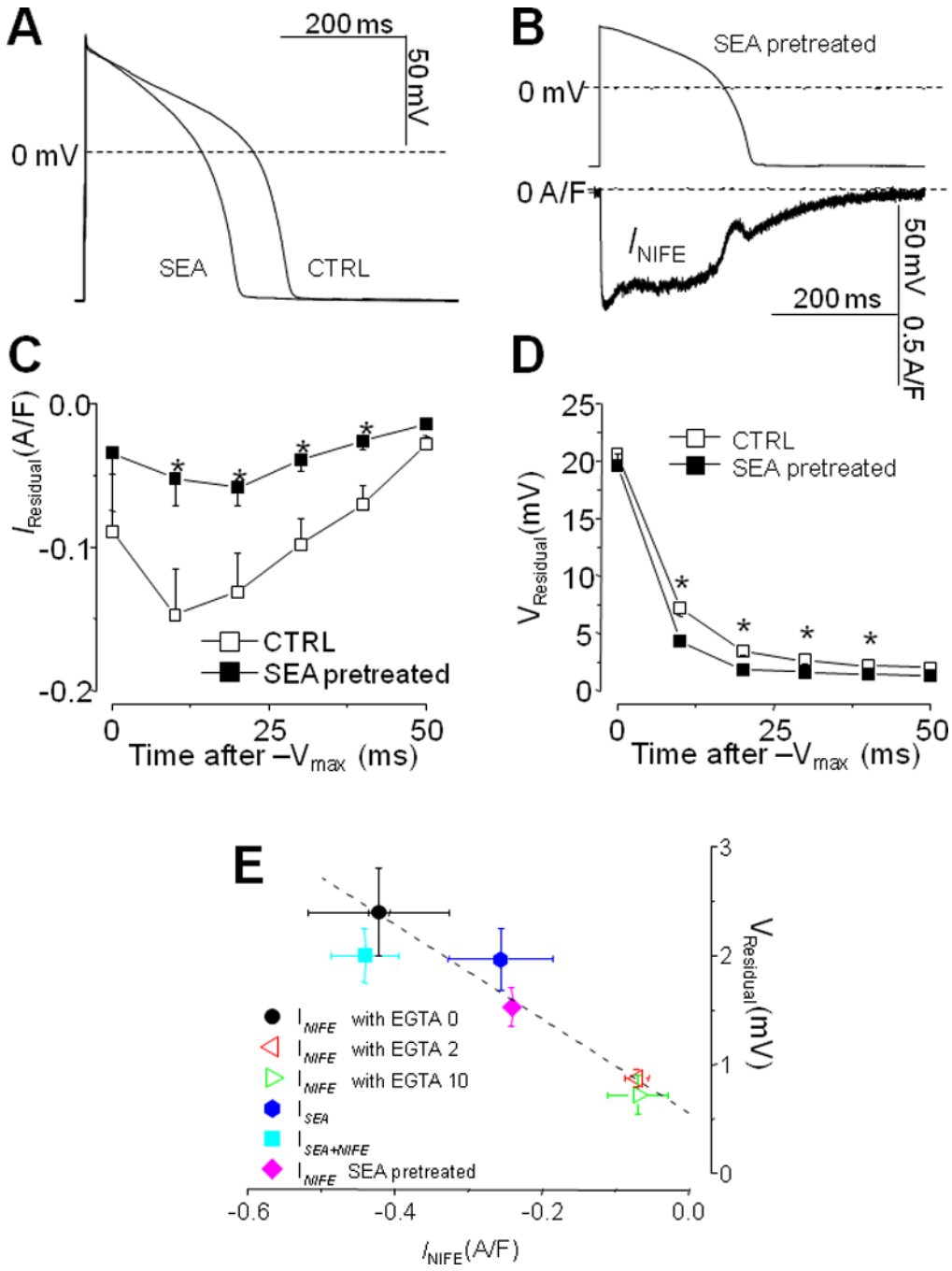

Fig.5.

Using 3 μM SEA0400 to treat cells shortened AP duration (A) and reduced I_{NIFE} (B). The residual current (C) and the residual depolarization (D) were significantly reduced (n=7 cells, t-test, $p<0.05$*), demonstrating a predominant influence of I_{NCX} on these features. Panel E shows a universal correlation (R=0.917) between the magnitude of residual current and residual depolarization under all experimental conditions tested.

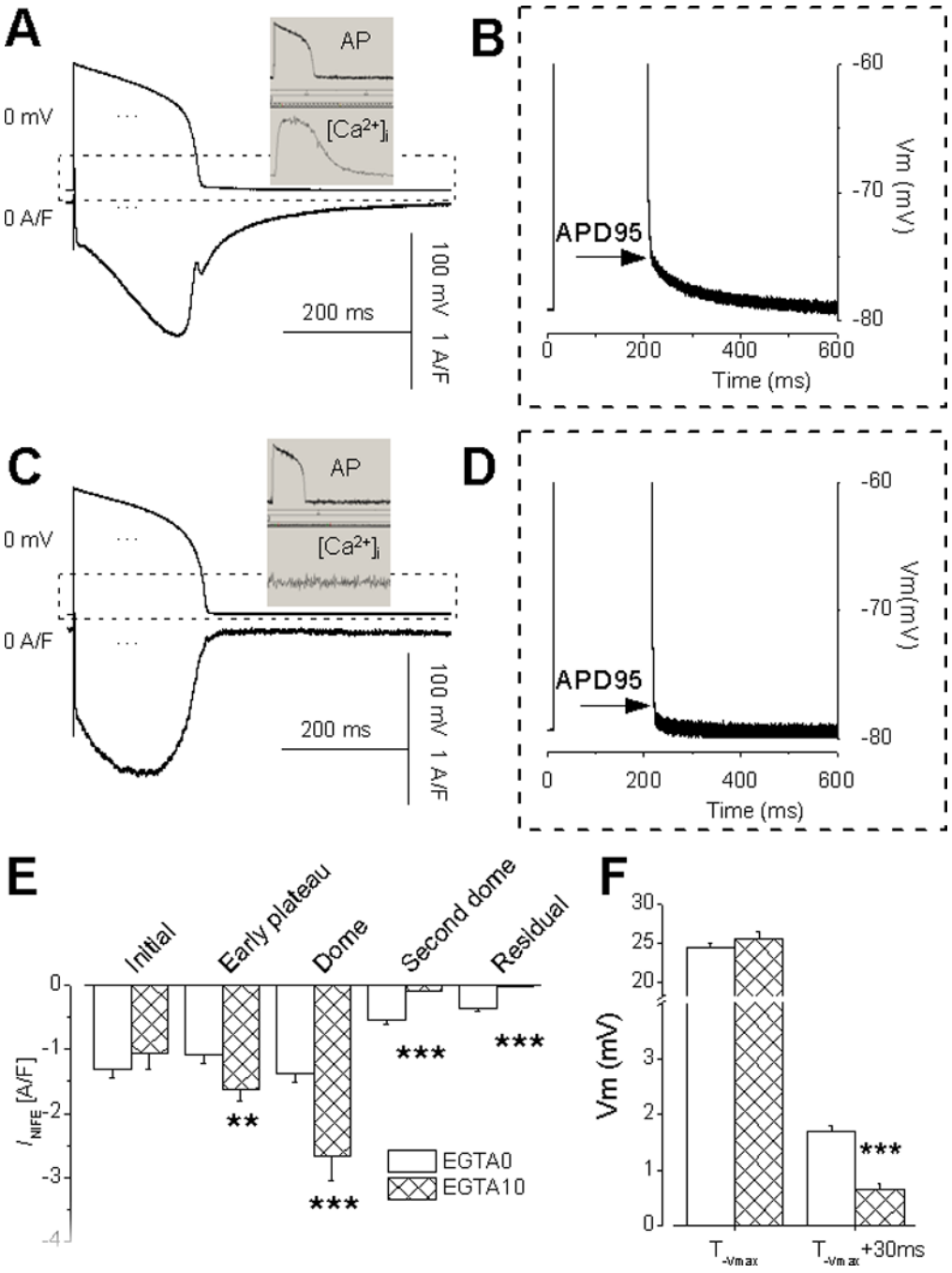

Fig.6.

These experiments were conducted at 36°C. Panel A shows a representative I_{NIFE} recorded under AP-clamp with Ca^{2+} cycling (n=19 cells). Notice the presence of the second dome and the residual current (A) and the residual depolarization (B). The insert shows the Ca^{2+} transient measured with Fura-2. Panel C shows a representative I_{NIFE} recorded with 10 mM EGTA (n=9 cells). Notice the absence of the residual current (C) and the residual depolarization (D). Panel E and F show the Mean ±SE and statistical comparison at the features points. (t-test $p<0.01$**, $p<0.001$***)

Table-1

Currents (pA/pF)	Ca^{2+} cycling (0 EGTA)	Ca^{2+} buffered (EGTA 10 mM)
I_{K1}	Ba^{2+} 50 µmol/L	
Diastolic	0.306 ±0.305	0.281 ±0.215
Peak	1.860 ±0.386	1.723 ±0.541
I_{Ks}	Chromanol-293B 10 µmol/L	
Diastolic	0.016 ±0.064	−0.007 ±0.138
Peak	0.340 ±0.219	0.374 ±0.208
I_{Kr}	E4031 1 µmol/L	
Diastolic	0.038 ±0.031	0.004 ±0.110
Peak	0.571 ±0.161	0.724 ±0.184*
I_{NIFE}	Nifedipine 10 µmol/L	
Diastolic	0.072 ±0.151	0.103 ±0.274
Peak	−1.434 ±0.302	−2.36 ±0.262***

Student's t-test p<0.05*

p<0.001*** (n=11–17 cells/group)